

# Room temperature spin coherence in ZnO

S. Ghosh, V. Sih, W. H. Lau, and D. D. Awschalom\*  
*Center for Spintronics and Quantum Computation,  
University of California, Santa Barbara, CA 93106*

S.-Y. Bae and S. Wang  
*Department of Materials Science and Engineering, Stanford University, Stanford, CA 94305*

S. Vaidya and G. Chapline  
*Lawrence Livermore National Laboratory, Livermore, CA 94550*  
(Dated: September 5, 2018)

Time-resolved optical techniques are used to explore electron spin dynamics in bulk and epilayer samples of  $n$ -type ZnO as a function of temperature and magnetic field. The bulk sample yields a spin coherence time  $T_2^*$  of 20 ns at  $T = 30$  K. Epilayer samples, grown by pulsed laser deposition, show a maximum  $T_2^*$  of 2 ns at  $T = 10$  K, with spin precession persisting up to  $T = 280$  K.

A lot of attention has been focused on zinc oxide (ZnO) because of material properties that make it well-suited for applications in ultra-violet light emitters, transparent high-power electronics and piezoelectric transducers. In addition, the theoretical work of Dietl *et al.*,<sup>1</sup> predicting room temperature ferromagnetism for Mn-doped  $p$ -type ZnO, has revealed the possibility that ZnO may be an appropriate candidate for spintronics.<sup>2</sup> The magnetic properties of thin films of ZnO with transition ion doping,<sup>3,4,5</sup> are being widely investigated, but practical spintronics applications would also require long spin coherence time and spin coherence length.

In this letter, we investigate the electron spin dynamics of non-magnetically doped  $n$ -type ZnO. The growth of  $p$ -type films is an experimental challenge, possibly due to self-compensation from oxygen vacancies<sup>6</sup> or the incorporation of hydrogen as an unintentional donor.<sup>7</sup> Consequently, recent developments reporting magnetic properties in ZnO have been regarding  $n$ -type samples,<sup>8</sup> although the preparation of  $p$ -type films has been reported.<sup>9,10</sup> Our measurements on  $n$ -type ZnO establish a spin coherence time of  $\sim 190$  ps at room temperature, longer than the spin coherence time reported in GaN,<sup>11</sup> another wide band-gap semiconductor. ZnO also has the added advantage that high quality single crystals are commercially available.

We concentrate on four samples - three 100 nm epitaxial thin films (designated samples A - C) and a bulk sample D. The thin films are fabricated by a pulsed laser deposition system using a ceramic ZnO pellet (Praxair Targets, Inc.) as the target and  $c$ -cut sapphire as the substrate, which is heated to 800°C during deposition. The substrate  $ab$  plane is rotated by 30 degrees with respect to that of the epilayers to reduce the lattice mismatch from 16 % to 3.85 %. Four-circle X-ray diffractometry confirms the single phase growth and the wurtzite structure of ZnO. The oxygen pressure used during the growth process for the epilayers is  $10^{-5}$  torr (sample A),  $10^{-4}$  torr (B) and  $10^{-3}$  torr (C), which tunes the carrier concentration. Sample D (commercial single crystal

from Tokyo-Denpa Company Ltd. grown by hydrothermal method<sup>12</sup>) is mounted on fused silica and polished down to a few microns for transmission measurements.

Transport measurements performed at room temperature show  $n$ -type conductivity in all four samples. The carrier concentrations (mobilities) for A - D are  $1.92 \times 10^{19} \text{ cm}^{-3}$  ( $19 \text{ cm}^2/\text{Vs}$ ),  $1.01 \times 10^{19} \text{ cm}^{-3}$  ( $27 \text{ cm}^2/\text{Vs}$ ),  $2.64 \times 10^{18} \text{ cm}^{-3}$  ( $37 \text{ cm}^2/\text{Vs}$ ), and  $1.26 \times 10^{15} \text{ cm}^{-3}$  ( $240 \text{ cm}^2/\text{Vs}$ ), respectively. We note that sample D has a carrier concentration several orders of magnitude smaller than the epilayers and a higher mobility.

Time-resolved Faraday rotation (TRFR), an optical pump-probe spectroscopic technique,<sup>13,14</sup> is used to probe the electron spin dynamics. A circularly-polarized pump pulse, incident normal to the sample surface, injects spin-polarized electrons, and the Faraday rotation angle of a linearly polarized probe pulse, applied after a time delay  $\Delta t$ , measures the projection of the electron spin magnetization as it precesses in a plane perpendicular to the applied transverse magnetic field (Voigt geometry). The pump and probe are typically tuned to 369 nm to address the band-gap of ZnO, using the frequency-doubled output from a mode-locked Ti:Sapphire laser with pulse duration  $\sim 150$  fs and repetition rate of 76 MHz ( $t_{rep} = 13$  ns). The laser beams are focused to a spot size of  $\sim 50 \mu\text{m}$ , and typical pump and probe powers are 1.9 mW and 200  $\mu\text{W}$ , respectively. The circular polarization of the pump beam is modulated with a photoelastic modulator at 50 kHz for lock-in detection.

TRFR results for samples A - C at  $T = 5.5$  K and  $B = 0.5$  T are shown in Fig. 1. The oscillatory component of the Faraday rotation  $\theta_F$  as a function of time delay is:

$$\theta_F(\Delta t) = A \exp(-\Delta t/T_2^*) \cos(\omega_L \Delta t) \quad (1)$$

where  $A$  is the amplitude of the electron spin polarization injected perpendicular to  $B$ ,  $T_2^*$  the transverse coherence time and  $\omega_L$  the Larmor frequency which is related to the electron  $g$ -factor  $g^*$  by  $\hbar\omega_L = g^* \mu_B B$  (where  $\mu_B$  is the Bohr magneton). Fits to the data in Fig. 1(a) indicate

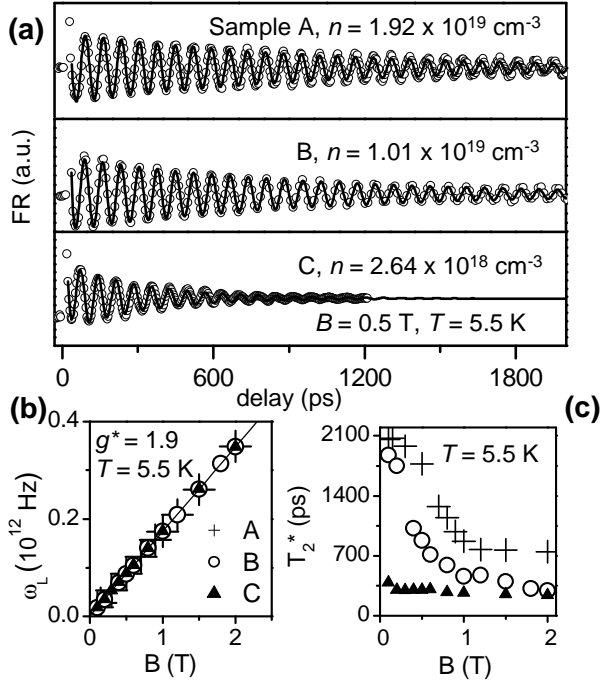


FIG. 1: (a) Time-resolved Faraday rotation as a function of pump-probe delay for samples A - C at  $T = 5.5 \text{ K}$  and  $B = 0.5 \text{ T}$ . The carrier densities are indicated in the figure. Lines are fits using eq. (1). (b) Larmor frequency  $\omega_L$  as a function of  $B$ . Line is a linear fit. (c) Spin coherence time  $T_2^*$  as a function of  $B$ . The symbols in (c) correspond to those in (b).

that  $T_2^*$  increases with increasing carrier concentration in the epilayers, from 0.5 ns (sample C) to 2.1 ns (sample A).

Figures 1(b) and (c) show the  $B$  - dependence of  $\omega_L$  and  $T_2^*$ , respectively. In Fig. 1(b),  $\omega_L$  increases linearly with  $B$  in all the samples (including sample D, not shown here) and we extract a field-independent value of  $g^* = 1.9$  for the three epilayers, consistent with earlier electron spin resonance (ESR) measurements.<sup>15</sup> This value of  $g^*$  is lower than that measured in the bulk sample D ( $g^* = 2.03$ ), which may be attributed to the in-plane compressive strain in the epilayers due to the lattice mismatch with the substrate. Figure 1(c) shows  $T_2^*$  decreasing by almost 60% when the magnetic field is increased from  $B = 0.1 \text{ T}$  to  $1 \text{ T}$  for samples A and B, and by about 30% for sample C. This field dependence is similar to that observed in GaN.<sup>11</sup>

In Fig. 2, we perform a detailed study of the temperature dependence of  $T_2^*$  in sample A, which has the highest carrier density, and the longest spin coherence time of all the epilayers. Figure 2(a) shows the TRFR response at  $B = 0.8 \text{ T}$  for temperatures  $T = 80 \text{ K}$ ,  $180 \text{ K}$  and  $280 \text{ K}$ . The  $g$ -factor  $g^*$  is temperature independent, while  $T_2^*$  decreases with increasing  $T$ . Remarkably, spin coherence persists until room temperature, with a spin lifetime of 188 ps at  $280 \text{ K}$ , considerably longer than the spin coherence time observed in GaN ( $\sim 35 \text{ ps}$ ).<sup>11</sup> Figure

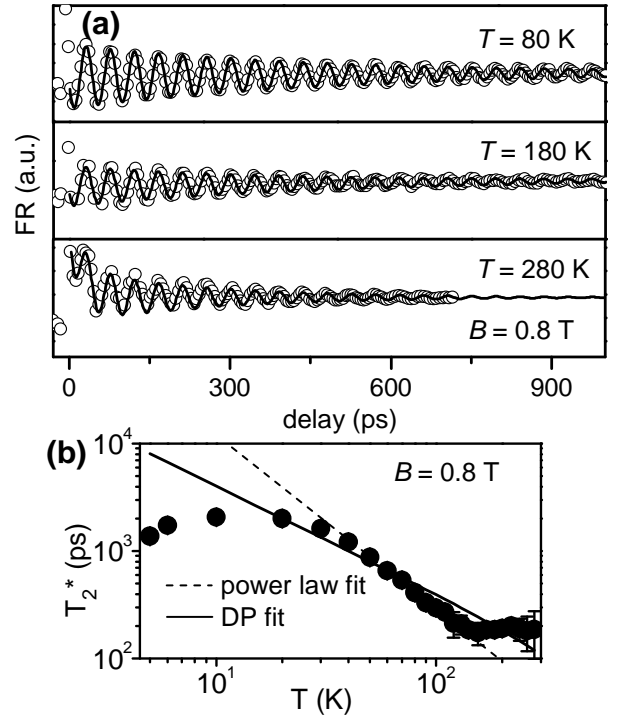


FIG. 2: Temperature dependence of TRFR on sample A. (a) Spin precession at three temperatures for  $B = 0.8 \text{ T}$ . (b)  $T_2^*$  follows a power law (dashed line) with temperature in the intermediate region of 30 to 150 K, with an exponent  $-1.54 \pm 0.03$ . Theoretical fit to the data for DP mechanism is shown as a solid line.

2(b) is a logarithmic plot of  $T_2^*$  obtained from TRFR data at  $B = 0.8 \text{ T}$ , as a function of  $T$ . For  $5.5 \text{ K} \leq T \leq 30 \text{ K}$ ,  $T_2^*$  is weakly temperature dependent, remaining almost constant at 2 ns; for  $30 \text{ K} \leq T \leq 150 \text{ K}$ , it follows a power law  $T^{-\alpha}$ , with  $\alpha = 1.54 \pm 0.03$ ; for  $150 \text{ K} \leq T \leq 290 \text{ K}$ , it is relatively flat, fluctuating around 190 ps.

TRFR data at  $T = 5 \text{ K}$  and  $B = 0.5 \text{ T}$  for the bulk sample D is shown in Fig. 3(a). We observe that the Faraday signal exhibits oscillations at negative delay, indicative of spin magnetization persisting from the previous laser pulse, suggesting  $T_2^* \geq t_{rep}$ . We employ the method of Resonant Spin Amplification (RSA) which makes it possible to measure spin coherence times well in excess of  $t_{rep}$ .<sup>16</sup> Here, the Faraday rotation is measured at a fixed pump - probe delay. By varying the magnetic field, and thus, the Larmor frequency, resonant enhancements in Faraday rotation occur when the spin precession and pulse repetition periods are commensurate, due to constructive interference of successively excited spin packets.

Figure 3(b) shows multiple RSA peaks in a magnetic field scan from  $+10 \text{ mT}$  to  $-10 \text{ mT}$  at  $\Delta t = 50 \text{ ps}$  and  $T = 30 \text{ K}$ . From a Lorentzian fit to the zero-field resonance peak, we obtain a  $T_2^*$  of 20 ns. Figure 3(c) shows a log-log plot of the temperature dependence of  $T_2^*$  in the bulk sample obtained from such fits for  $5 \text{ K} \leq T \leq$

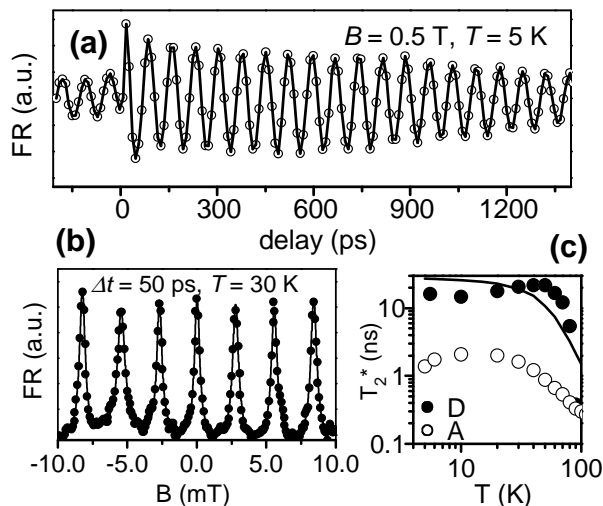


FIG. 3: (a) TRFR at  $T = 5$  K for the bulk sample D. Line is a guide to the eye. (b) Faraday rotation versus  $B$  at  $T = 30$  K and  $\Delta t = 50$  ps on sample D showing multiple RSA peaks. Lines are fits to data. (c)  $T_2^*$  obtained from RSA peak at  $B = 0$  T, as a function of temperature for sample D (filled circles) with data from sample A (open circles) shown for comparison. The line is a theoretical fit of the DP mechanism for sample D.

100 K. For comparison, we reproduce the temperature dependence of sample A from Fig. 2(b), and notice that despite having carrier concentration four orders in magnitude lower,  $T_2^*$  is larger by a factor of ten in the bulk. It also does not follow the power law of  $T^{-3/2}$  seen in the epilayer. We speculate that these differences between the bulk and the epilayer may be attributed to the presence of compressive strain and higher density of defects in the

latter.

Of the three spin decoherence mechanisms relevant in semiconductors - Elliot-Yafet (EY),<sup>17</sup> D'yakonov-Perel (DP),<sup>18</sup> and Bir-Aronov-Pikus (BAP)<sup>19</sup> mechanisms, the EY process should not be very efficient in ZnO due to its large band-gap and small spin-orbit splitting,<sup>20</sup> while the BAP process should only make a significant contribution to the spin relaxation rate when the concentration of holes is high ( $\sim 10^{17}$  cm<sup>-3</sup>). We show in Fig. 2(b) and 3(c) (solid lines) the electron spin relaxation rate for the DP process, calculated using

$$[T_2^{-1}]_{DP} = \frac{24m_e^*\gamma_1^2k_B T\tau_{tr}}{\hbar^4} + \frac{256(m_e^*)^3\gamma_3^2E_g(k_B T)^3\tau_{tr}}{21\hbar^6}. \quad (2)$$

where<sup>21</sup>  $m_e^*$  is the electron effective mass,  $E_g$  the band gap,  $\gamma_1$  and  $\gamma_3$  the spin-splitting coefficients and  $\tau_{tr}$  is the transport time, related to the mobility  $\mu$  via  $\tau_{tr} = \mu m_e^*/q$  ( $q$  is the electron charge). While it predicts the correct qualitative trends, it does not explain all the data, especially the persisting spin coherence at high temperatures, suggesting that there may be other spin scattering processes responsible for our findings.

In conclusion, we have studied spin coherence in bulk and epilayer samples of ZnO. In the bulk sample,  $T_2^*$  extends to very long times at low temperatures. In the epilayers,  $T_2^*$  increases with carrier concentration, but is much smaller than in the bulk. However, spin precession in the epilayers persist until room temperature, adding to the attractiveness of ZnO as a material for spintronics.

We thank R. J. Epstein and Y. K. Kato for discussions and AFOSR, ARO, ONR and DARPA/DMEA for financial support.

\* Electronic address: awsch@physics.ucsb.edu  
<sup>1</sup> T. Deitl, H. Ohno, F. Matsukura, J. Cibert, and D. Ferrand, *Science* **287**, 1019 (2000).  
<sup>2</sup> S. A. Wolf, D. D. Awschalom, R. A. Buhrman, J. M. Daughton, M. L. Von Molnar, S. Roukes, A. Y. Chtchelkanova and D. M. Treger, *Science* **294**, 1488 (2001).  
<sup>3</sup> S. J. Pearton, D. P. Norton, K. Ip, Y. W. Heo, and T. Steiner, *J. Vac. Sci. Technol. B* **22**(3), 932 (2004).  
<sup>4</sup> S. W. Jung, S. J. An, G. C. Yi, C. U. Jung, S. I. Lee, and S. Cho, *Appl. Phys. Lett.* **80**, 4561 (2002).  
<sup>5</sup> T. Fukumura, Z. Jin, M. Kawasaki, T. Shono, T. Hasegawa, S. Koshihara, and H. Koinuma, *Appl. Phys. Lett.* **78**, 958 (2001).  
<sup>6</sup> D. C. Look, J. W. Hemsky, and J. R. Sizelove, *Phys. Rev. Lett.* **82**, 2552 (1999).  
<sup>7</sup> C. G. Van de Walle, *Phys. Rev. Lett.* **85**, 1012 (2000).  
<sup>8</sup> K. Ueda, H. Tabata, and T. Kawai, *Appl. Phys. Lett.* **79**, 988 (2001).  
<sup>9</sup> K. Minegishi, Y. Koiwai, Y. Kikuchi, K. Yano, M. Kasuga, and A. Shimizu, *Japan. J. Appl. Phys.* **36**, L1453 (1997).  
<sup>10</sup> V. Vaithianathan, B. T. Lee, and S. S. kim, *Appl. Phys. Lett.* **86**, 062101 (2005).

<sup>11</sup> B. Beschoten, E. Johnston-Halperin, D. K. Young, M. Poggio, J. E. Grimaldi, S. Keller, S. P. DenBaars, U. K. Mishra, E. L. Hu, and D. D. Awschalom, *Phys. Rev. B* **63**, 121202(R) (2001).  
<sup>12</sup> N. Sakagami and K. Shibayama, *Japan. J. of App. Phys.* **20**, 201 (1981).  
<sup>13</sup> S. A. Crooker, D. D. Awschalom, J. J. Baumberg, F. Flack and N. Samarth, *Phys. Rev. B* **56**, 7574 (1997).  
<sup>14</sup> S. A. Crooker et al., *Phys. Rev. Lett.* **77**, 2814 (1996).  
<sup>15</sup> P. Kasai, *Physical Review* **130**, 989 (1963).  
<sup>16</sup> J. M. Kikkawa and D. D. Awschalom, *Phys. Rev. Lett.* **80**, 4313 (1998).  
<sup>17</sup> R. J. Elliot, *Phys. Rev.* **96**, 266 (1954).  
<sup>18</sup> M. I. D'yakonov and V. I. Perel', *Sov. Phys. JETP* **42**, 7905 (1976).  
<sup>19</sup> G. L. Bir, A. G. Aronov, and G. E. Pikus, *Sov. Phys. JETP* **42**, 705 (1976).  
<sup>20</sup> O. Madelung, "Semiconductors: Data Handbook", Springer 2003.  
<sup>21</sup> The parameters used in the calculations for  $[T_2]_{DP}$  in the epilayers are  $\gamma_1 = 0.005$  eV $\text{\AA}$ ,  $\gamma_3 = 5$  eV $\text{\AA}^3$ ,  $m_e^* = 0.275 m_e$ , and  $E_g = 3.445$  eV. In the epilayer, the measured mobility

is temperature independent and for the calculation we use  $\mu(20\text{K}-280\text{K})=19 \text{ cm}^2/\text{Vs}$ , for evaluating  $\tau_{tr}$ . In the bulk we use the measured values for the temperature-dependent

mobility  $\mu$ , and tune  $\gamma_1$  to  $0.5 \text{ meV}\text{\AA}$ , to account for the decreased strain compared to the epilayers.